Molecular Insights for Alzheimer's Disease: An Unexplored Storyline on the Nanoscale Impact of Nascent Aβ 1–42 toward the Lipid Membrane

David Siniscalco, Grégory Francius, Mounir Tarek, Semiha Kevser Bali, Olivier Laprévote, Catherine Malaplate-Armand, Thierry Oster, Lynn Pauron, Fabienne Quilès

https://pubs.acs.org/doi/10.1021/acsami.2c22196

Molecular Insights for Alzheimer's Disease: an Unexplored Storyline on the Nanoscale Impact of Nascent $A\beta_{1-42}$ towards Lipid Membrane

*David Siniscalco[1], Grégory Francius[1], Mounir Tarek[2], Semiha Kevser Bali[2], Olivier Laprévote[2], Catherine Malaplate[3], Thierry Oster[3], Lynn Pauron[3,4], Fabienne Quilès[1]**

[1] Université de Lorraine, CNRS, LCPME, F-54000 Nancy, France

[2] Université de Lorraine, CNRS, LPCT, F-54000 Nancy, France

[3] Université de Lorraine, UR AFPA, F-54000 Nancy, France

[4] Université de Lorraine, CNRS, IMoPA, F-54000 Nancy, France

KEYWORDS: Alzheimer's disease, Amyloid β, Supported Lipid Bilayers, ATR-FTIR, AFM, Molecular Dynamics

ABSTRACT

Deciphering the mechanism of Alzheimer's disease is a key element for designing an efficient therapeutic strategy. Molecular dynamics (MD) calculations, atomic force microscopy and infrared spectroscopy were combined to investigate β-amyloid ($A\beta_{1-42}$) peptide interactions with supported lipid bilayers (SLBs). The MD simulations showed that nascent $A\beta_{1-42}$ monomers remain anchored within a model phospholipid bilayer's hydrophobic core, which suggests their stability in their native environment. We tested this prediction experimentally, by studying the behavior of $A\beta_{1-42}$ monomers and oligomers when interacting with SLBs. When $A\beta_{1-42}$ monomers and oligomers were self-assembled with lipid bilayer and deposited as SLB, they remain within the bilayers. Their presence in the bilayers induces destabilization of the model membranes. No specific interactions between $A\beta_{1-42}$ and the SLBs were detected when SLBs free of $A\beta_{1-42}$ were exposed to $A\beta_{1-42}$. This study suggests that Aβ can remain in the membrane after cleavage by the γ-secretase, and cause severe damage in the membrane.

INTRODUCTION

Alzheimer's disease (AD) is a widespread neurodegenerative disease, which was described primarily with the presence of extracellular amyloid plaques in the brain[1] often composed of β-amyloid peptides (Aβ, 37 to 43 amino acids),[2] one of its pathological hallmark signatures. The production of Aβ from its amyloid-peptide precursor protein (APP) occurs in membrane micro-domains where APP is co-segregated with the β- and the γ-secretases.[3] APP undergoes first an extracellular proteolysis by β-secretase, producing CTFβ (C99) and a soluble APP-β fragments.[4] The production of Aβ results from the subsequent regulated intramembrane proteolysis of the CTFβ transmembrane α-helix, the γ-secretase complex, occurring mostly in early endosomes.[5-7] This amyloidogenic pathway competes with a physiological one that involves APP proteolysis by α-secretase and γ-secretase, leading to the generation of a neurotrophic sAPPα and p3 fragments. Membrane remodeling and anomalies in raft composition/organization are thought to be linked to neurodegeneration and higher susceptibility to AD in aging individuals.[3, 8]

It is commonly accepted (current hypothesis) that nascent Aβ peptides are immediately expelled from the membrane after proteolysis of CTFβ, then becoming neurotoxic to other cell membranes upon oligomerization (Figure 1a) though the precise role of $A\beta_{1-42}$ oligomers is not fully understood.[2, 9] Reference to the physicochemical factors that influence the interactions between the lipid membrane environment and the protein actors involved in APP proteolysis or those driving the expulsion of Aβ peptides from the membrane is lacking.[10] The processes at play in the amyloidogenic pathway are modulated by several key membrane components: cholesterol for instance is known to bind to APP to regulate its membrane insertion[11] and to facilitate its processing into Aβ in the dynamic platforms composed by lipid rafts that reorganize thanks to specific protein-protein and protein-lipid interactions.[12]

Several studies of non-neural cellular systems have shown indeed that amyloid peptide is produced in endosomes which are cellular compartments characterized by acidic media, optimal for γ-secretase activity.[6] The endosomal membrane is thus a confirmed site of Aβ peptide production, *i.e.* the site where the pathological pathway responsible for AD takes place.[7] After the proteolysis of CTFβ by γ-secretase within the lipid bilayer, the Aβ produced probably adopts a helical conformation.[13] Among the monomeric or aggregated $A\beta_{1-42}$ structures deposited at the Protein Data Bank,[14] almost all correspond to hypothetical models of "secreted" Aβ: The 2LLM and 2LOH structures present the APP transmembrane α-helix in monomeric and dimeric forms inserted in a detergent micelle with hydrophobic domains (surfactant tail lengths) comparable to that of biological bilayer lipids.[15] Furthermore, Aβ peptides can interact with each other in the membrane upon γ-secretase-processing of CTFβ[16] and oligomerize while still anchored in the membranes. Several arguments are in favor of the intracellular membrane production and aggregation of Aβ. A very recent *in vitro* study elegantly demonstrated also in various biomimetic model organelle membranes that $A\beta_{1-42}$ aggregation kinetics is influenced by lipid composition, especially in the inner endosomal leaflet comparable to the outer leaflet of the plasma membrane.[17] In addition, numerous works have described the very high affinity of oligomeric Aβ peptide for membranes and membrane lipids, but without describing consensually the types of interactions.[18] In differentiated PC12 cells and in N2a cells stably expressing APPswe and PS1, $A\beta_{1-42}$ peptide was also found tightly associated with the lysosomal membrane, while the proportion in the lysosomal lumen is minimal.[19] Both in cell models and in AD patient brains, oligomeric Aβ peptide is found in neuronal exosomes, extracellular vesicles secreted downstream of the endosomal trafficking system, which could represent a prion-like mode of propagation of the amyloidopathy in AD.[20] This led us to question the relevance of the hypothesis considering that the Aβ peptide is expelled from an environment despite having a high affinity for it to the point of returning

to it after being secreted and possibly oligomerized. We propose here to consider a new hypothesis that at least a fraction of Aβ may remain anchored in the membrane after its proteolysis. This incited us to reconsider some of the weakest paradigms with the aim of improving knowledge of the molecular mechanisms involved, especially the earliest ones that occur at the membrane level. We initially investigated the outcome of the APP precursor by carrying out atomistic molecular dynamics (MD) simulations of "nascent" Aβ peptide homologs in model lipid bilayers. The work presented in this paper entailed modeling the transmembrane domain (TMD) of APP, as well as its proteolytic products. As our data show, simulations of non-proteolyzed dimeric TMD revealed a relatively stable dimer that remains inserted in the model membranes. Likewise, $A\beta_{1-42}$ monomers representing the cleaved APP remained also stably anchored within the model membrane hydrophobic core, indicating rather their stability in their native environment. We therefore tested these predictions using a host of spectroscopic analytical techniques, studying Aβ and their behavior in model membranes namely supported lipid bilayers (SLBs).

SLBs are widely used as model systems to mimic biological membranes, and their physicochemical features can be compared easily with those of cell membranes.[21-22] They can be investigated with several techniques, including atomic force microscopy (AFM), a powerful method for deciphering nanoscale biological and biophysical phenomena such as peptide–membrane interactions.[23-24] Interestingly AFM is the only technique allowing high-resolution imaging, *in situ* and real-time monitoring of SLBs in physiological environment, and determination of surface features.[25] Furthermore, it is a relevant tool for detection and observation of peptide aggregation in membranes,[24] and it has been shown to be useful in studying Aβ peptides-membrane interactions.[24, 26-31] Attenuated total reflectance Fourier transform infrared spectroscopy (ATR-FTIR) is a strong complementary technique providing structural, conformational and biochemical features of SLBs *in situ* and under physiological

conditions.[32] ATR-FTIR spectroscopy is especially relevant in deciphering lipid–peptide interactions and any conformational change of Aβ peptides.[27, 33] These measurements are relevant to unravel possible self-organization/oligomerization of the $A\beta_{1-42}$ peptides in interaction with the SLB and provide further information on the phospholipid organization.[32, 34] Furthermore, dichroic ratios (R^{ATR}) and the corresponding order parameters (S_L) of selected vibrational modes can be used to obtain information on the organization of SLBs,[35-36] and the impact the Aβ peptides' presence might have on them. The spatial scales of both methods are different: AFM provides a local information on the SLB from about a few hundred nm^2 to a few tens μm^2, whereas ATR-FTIR provides average information on the whole SLB on the ATR crystal (7 mm^2 in this study).

With one exception, AFM and ATR-FTIR studies published so far focused on investigating the effect of various "secreted" forms of Aβ in which soluble Aβ species are added to preformed SLBs with variable protocols for preparation of Aβ peptide.[24, 37] Several studies demonstrate monomeric or oligomeric Aβ species' preference for interaction with bilayers rich in 1,2-dioleoyl-sn-glycero-3-phospho-*rac*-(1-glycerol) (DOPG), 1,2-dipalmitoyl-sn-glycero-3-phosphocholine (DPPC), phosphatidylserine, or ganglioside GM1.[38] They reveal different degrees and morphologies of aggregation on the surface of bilayers and degradation of bilayer structure. One common factor among these studies is the propensity of bilayers to either trigger or accelerate Aβ aggregation. Although most of the considered model membranes are composed of one lipid species, a few include multi-lipid bilayer compositions.[38-39]

The present work characterizes two putative models of $A\beta_{1-42}$ alteration of membranes: the classical "secreted" model in which we study the effect of addition of oligomers of Aβ peptide onto pre-formed lipid bilayers, and a novel "nascent" model, in which we study the effect of incorporation of a membrane-primed Aβ peptide during the formation of the lipid

bilayer. We investigate hence an alternative hypothesis related to the amyloid cascade according to which a part of the $A\beta_{1-42}$ peptides in monomer form might stay in the membrane after the two steps of APP hydrolysis, and aggregate *in situ* presenting ultimately a toxic effect (Figure 1b).

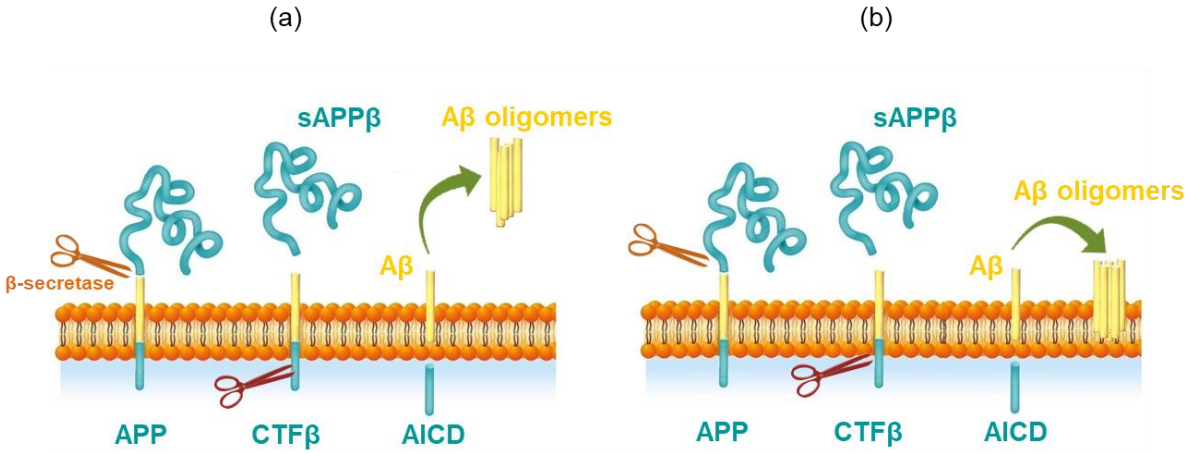

Figure 1. (a) Schematic representation of the classic proteolytic process of APP, leading to the amyloid cascade hypothesis. (b) An alternative hypothesis: nascent Aβ peptide remains inserted in the membrane and Aβ peptide makes oligomers inside the membrane.

RESULTS

$A\beta_{1-42}$ remains embedded within a phospholipid bilayer in MD simulations.

We built a putative nascent structure of $A\beta_{1-42}$ embedded in a phospholipid bilayer using an APP juxtamembrane-transmembrane (APPjmtm) structure as a template.[15] Note that this initial $A\beta_{1-42}$ structure presents an extramembrane N-terminal part and transmembrane with an α-helix, one extra- and one transmembrane, separated by a loop spanning residues Val24 to Lys28, analogous to one monomer of 2LOH. Microsecond-long atomistic MD simulations performed with one, two and four $A\beta_{1-42}$ embedded in a phospholipid bilayer of DOPC showed that the transmembrane segment of the peptides remains in its helical form and anchored in the lipid bilayer (Figure 2).

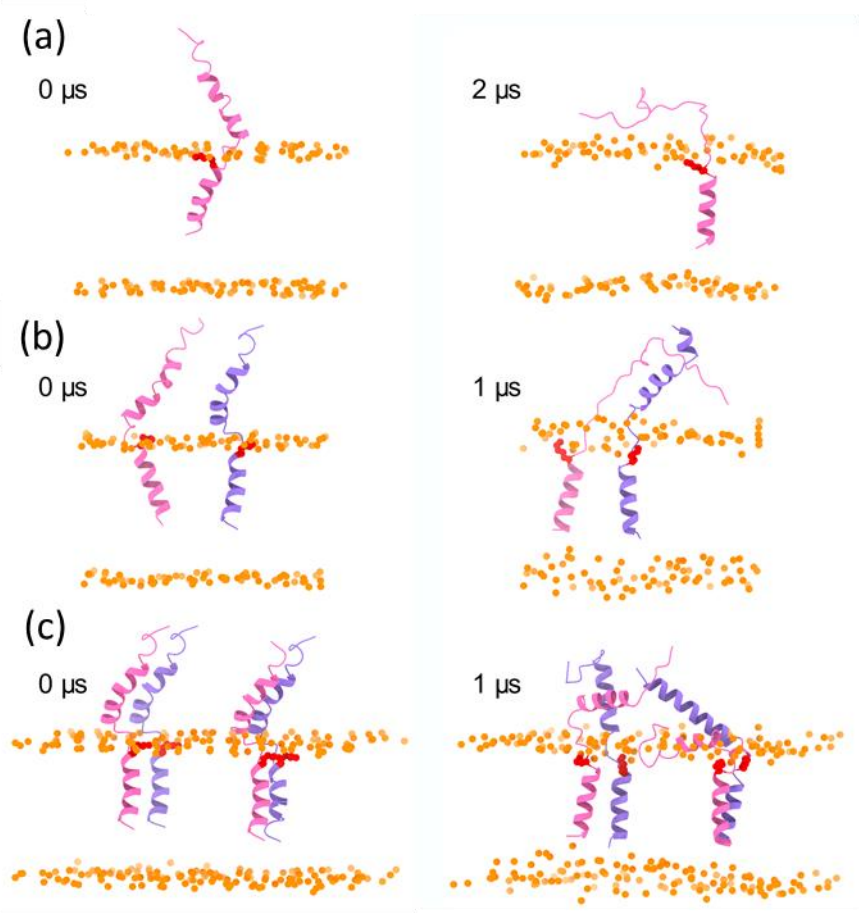

Figure 2. Molecular dynamics study of helical Aβ peptide anchored in membrane at initial state and last frame of systems containing (a) one monomer, (b) two monomers and (c) four monomers. Yellow: phosphorus atoms of DOPC. Pink and blue: Aβ peptides. Lys28 is shown in red.

In monomeric simulations, the N-terminal of $A\beta_{1-42}$ unfolded and remained disordered through the rest of the simulation. Two and four $A\beta_{1-42}$ peptides interacting together also remain embedded in a DOPC lipid bilayer. In the case of two $A\beta_{1-42}$ peptides, four replicates of 1 µs were simulated with different orientations of the two dimers and all stay persistently anchored in the lipid bilayer (Figure 2b). Interestingly, in these simulations the α-helical secondary structure of extracellular N-terminal remains stable in six out of eight peptides. Contrarily to the NMR structure of micellar APPjmtm (2LOH), two Aβ peptides initially placed near each other

were not found to interact through their transmembrane domains, and instead interacted extensively with their N-terminal extracellular domains.

$A\beta_{1-42}$ triggers local damages when included during SLBs formation.

We have analyzed the morphology and the spectroscopic properties of SLBs prepared from deposition of single unilamellar vesicles (SUVs) formed by assembly of lipids (POPC and DPPC at a 60/40% molar composition determined by ATR-FTIR, Figure S1a-b in Supplementary Information) suspended with respectively 0 µM (called POPC/DPPC), 20 µM or 50 µM $A\beta_{1-42}$ peptides[28] (called POPC/DPPC/$A\beta_{1-42}$). The choice of this lipid ratio was motivated by the fact that it is representative of biological membranes as it forms domains of liquid-like and domains of gel-like phases. The presence of these domains makes it as well easier to detect the SLB coverage with AFM. Note here that the SLBs were prepared by controlling the experimental conditions to ensure that $A\beta_{1-42}$ in solution are mostly under initial oligomeric or mostly monomeric forms (Figure S2).

In comparison to POPC/DPPC SLBs (Figure S1c), the high-resolution AFM images of POPC/ DPPC/$A\beta_{1-42}$ SLB for $A\beta_{1-42}$ oligomers (Figures 3a-c and S3) evidence some areas showing several defects and pores (~10-100 nm, black areas corresponding to the mica substrate) mainly located within the liquid phase, *e.g*. the POPC domains (dark areas) as well as cracks in the DPPC gel phase domains (bright areas). These features are further supported by the analyses of the corresponding cross-sections. They reveal typical height differences of 1-2 nm between the liquid-like and gel-like phases related to the POPC and DPPC domains, respectively, and noticeably heights of ~5 nm commonly attributed to the thickness of SLBs.[23] Most noticeably, Figure 3a-c evidence as well the presence of filamentous structures around the pores also distributed over the liquid-phase domains. The analysis of their height cross section revealed that these filamentous structures exhibit an average width of about 20 ± 1

nm[40] with a height difference with respect to the liquid phase membrane of about 0.7 ± 0.2 nm. These filamentous structures, 95.3 ± 61.3 nm long are, interestingly, characteristic of $A\beta_{1-42}$ protofibrils features in terms of size.[26, 41-42] Peak force tapping images provided qualitative information about mechanical properties of the SLBs according to the presence or absence of $A\beta_{1-42}$ peptides. Careful inspection of these images evidenced DMT moduli of about 9 and 12 MPa for POPC and DPPC domains, respectively. Besides, fibrous structures with values of about 7 MPa were observed mainly in the fluid POPC domains (Figure S4).

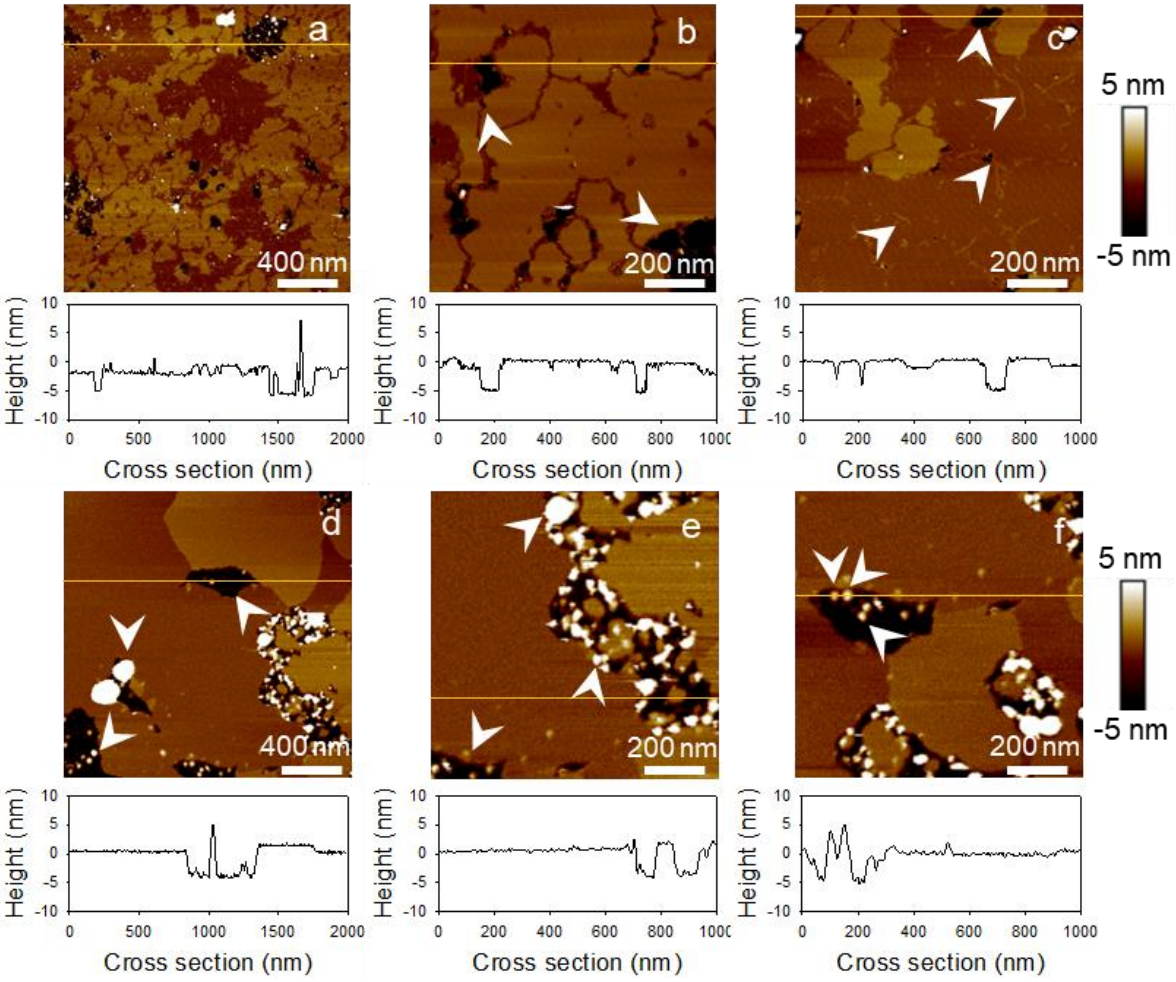

Figure 3. AFM topography images and corresponding cross-sections (at the yellow lines) of POPC/DPPC/$A\beta_{1-42}$ SLB, i.e. when $A\beta_{1-42}$ at 20 µM is included during the formation of the SLB. (a, b, c): $A\beta_{1-42}$ is mainly under oligomeric initial form. (d, e, f): $A\beta_{1-42}$ is mainly under monomeric initial form. Arrows show membrane degradation (pores or filaments in POPC

area). Cross sections are also indicated at the yellow lines, the 0 nm height is set at the top of the SLB.

For SLBs formed by ensuring the $A\beta_{1-42}$ in solution before assembly with lipids are mainly under monomeric form (Figure 3d-f), AFM analysis revealed similar defects and pores (~10-200 nm) as for the oligomeric form as described above. However, no filamentous structures were observed, but rather globular structures of ~40-100 nm diameter. Besides, the presence of cylindrical structures of >10 nm height for ~20 nm diameter was observed mainly in the pores, and also some protruding from the SLB (see cross section, Figure 3f). Such features could be attributed to $A\beta_{1-42}$ multimers as depicted in Figure 2.

ATR-FTIR spectra were used to monitor the time-evolution of the biochemical fingerprints of POPC/DPPC (control) and POPC/DPPC/$A\beta_{1-42}$ SLBs (Figure 4). The amide I band is very sensitive to peptide conformation, and it has been shown also for Aβ peptides.[33, 43-44] The inspection of ATR-FTIR spectra collected for 2 hours allowed detection of $A\beta_{1-42}$ oligomers through the very weak change in intensity in the amide band I region only with 50 µM of $A\beta_{1-42}$ (see spectral region in the grey rectangle in Figure 4b). The amide I band was observed at 1634 cm^{-1} and assigned to $A\beta_{1-42}$ β-sheets.[33, 43-44] When $A\beta_{1-42}$ monomers are considered, the ATR-FTIR spectra show clearly narrow amide I and II bands at 1653 and 1559 cm^{-1}, respectively (Figure 4c). These amide bands are assigned to α-helices.[45] These features suggested that the insertion of $A\beta_{1-42}$ monomers in the SLB was higher than that of $A\beta_{1-42}$ oligomers. The rinsing step with HEPES buffer did not remove significantly the peptide from the SLB.

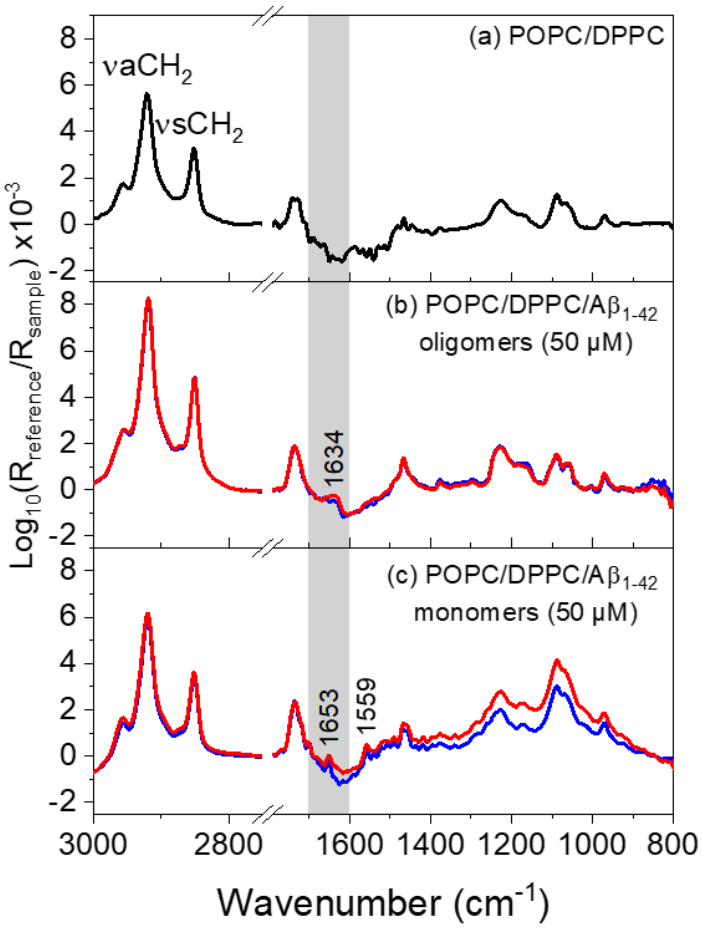

Figure 4. ATR-FTIR spectra of POPC/DPPC SLBs in the presence or absence of $A\beta_{1-42}$. (a) POPC/DPPC SLB; (b) POPC/DPPC/$A\beta_{1-42}$ (50 μM under oligomers initial form), and (c) POPC/DPPC/$A\beta_{1-42}$ (50 μM under monomer initial form) SLBs constructed with the initial presence of $A\beta_{1-42}$. The reference spectrum is the HEPES buffer. Red curves: before rinsing with HEPES buffer. Blue curves: after rinsing with HEPES buffer. ν: stretching, a: antisymmetric, s: symmetric. The grey rectangle is used to highlight the amide I band region in every spectrum.

Besides, dichroic ratios (R^{ATR}) and the corresponding order parameters (S_L) were calculated from the νsCH_2 bands for POPC/DPPC and POPC/DPPC/$A\beta_{1-42}$ SLBs for both forms of the peptide (Figure 4 and Table S1). S_L was slightly lower for POPC/DPPC/oligomeric-$A\beta_{1-42}$ (0.22 against 0.26 for POPC/DPPC SLB). S_L was drastically decreased when SLB

incorporated $A\beta_{1-42}$ monomers (0.26 to 0.09 from POPC/DPPC SLB to POPC/DPPC/$A\beta_{1-42}$ SLB). It strongly suggests a high disorder induced by the peptide inside the SLBs. Both S_L values indicated a loss of organization at different levels of the POPC/DPPC/$A\beta_{1-42}$ SLB with respect to POPC/DPPC SLB. This result is in accordance with AFM images showing a higher disorder in POPC/DPPC/$A\beta_{1-42}$ SLB with respect to POPC/DPPC SLB (Figures 3 and 5a).

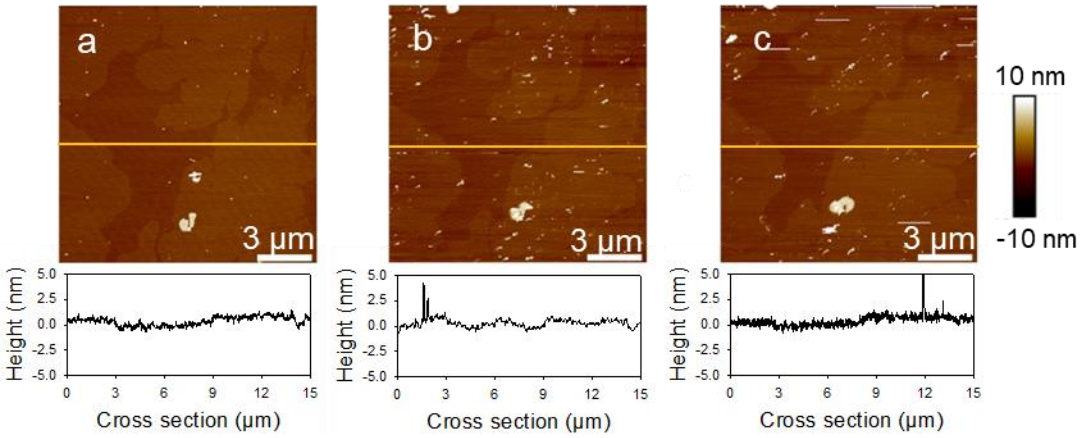

Figure 5. AFM topography images and corresponding cross-sections (at the yellow lines) of POPC/DPPC SLBs (60%/40%) upon addition of $A\beta_{1-42}$ at 20 µM mainly under oligomeric initial form (a, b, c). Tracking occurred during 2 hours: before exposure to $A\beta_{1-42}$ (a), exposed for 1 hour (b) and 2 hours (c). The set point of images was 0.4 nN (a, b) and 1.2 nN (c). The 0 nm height is set at the top of the SLB.

Free $A\beta_{1-42}$ oligomers in aqueous solution do not penetrate the SLBs.

At first sight, we are tempted to assign the presence of filaments to oligomerization of $A\beta_{1-42}$ peptides that remained well anchored within the lipid bilayers since the formation of the SUVs *i.e.* before their fusion onto the mica substrate to form SLBs. To confirm this, we need to check if potentially free $A\beta_{1-42}$ peptides remaining in the samples lead to similar assemblies when interacting with SLB. We carried out therefore the same experiments combining AFM

and ATR-FTIR to monitor the structural changes occurring when already formed pure lipid SLBs are exposed to µM solutions of free $A\beta_{1-42}$.

The beforehand prepared POPC/DPPC SLBs were exposed to solutions of $A\beta_{1-42}$ oligomers at concentrations of 20 (Figure 5) and 2.5 µM (data not shown). They were continuously imaged for 2 hours on the same area. At 2.5 µM $A\beta_{1-42}$, no significant changes in the morphology of the SLBs were observed as confirmed by the stable roughness of both phases measured at 0.3 ± 0.1 nm (Figure S5, Table S2). When the concentration of $A\beta_{1-42}$ oligomers was increased to 20 µM, a high accumulation or adsorption of aggregates was observed. Qualitatively, the latter exhibited increasing sizes with the exposure time (Figure 5b) and they may be associated to oligomers. The verification of this conclusion needs further spectroscopic analyses (see below). Noticeably, the vast majority of aggregates adsorbed on the gel phase domains of the SLB surface. Such high adsorption was supported by an increase of the gel-phase average roughness from 0.3 ± 0.1 nm up to 0.4 ± 0.1 nm (Table S2). After two hours exposure to free $A\beta_{1-42}$ oligomers, the membrane surface was scraped with increasing applied forces in order to roughly estimate the aggregates adherence or interactions with the SLBs. Interestingly, the applied shear force of *ca.* 1.2 nN was enough to remove all aggregates without damaging the membrane (Figure 5c). The statistical analysis of the morphological data for each phase did not evidence differences in SLBs roughness before and after exposure to $A\beta_{1-42}$ and scraping for all three concentrations of $A\beta_{1-42}$. These results indicate clearly that the $A\beta_{1-42}$ aggregates adsorbed loosely on the DOPC/DPPC SLB after its deposition on the bilayer surface.

ATR-FTIR fingerprints of beforehand formed SLBs (DOPC, DPPC and DOPC/DPPC) exposed to free $A\beta_{1-42}$ oligomers at 20 or 50 µM were monitored for 2 hours (Figures 6 and S6). The whole spectral time-evolution for both $A\beta_{1-42}$ concentrations appeared very similar. For all experiments, no changes were observed in the integrated intensities of νCH_2 stretching

modes. The amount of SLBs deposited on the ATR crystal did not change during exposure to $A\beta_{1-42}$. Integrated intensities ratios amide I/νC=O and amide II/νC=O increased during *ca.* 30 minutes and then reached a plateau. These features showed the approach of $A\beta_{1-42}$ to the vicinity of the SLB in every case, and the quantity of $A\beta_{1-42}$ present on pure DPPC SLB was higher than on pure POPC SLB, whereas DPPC/POPC SLB showed an intermediary feature (Figure S6).

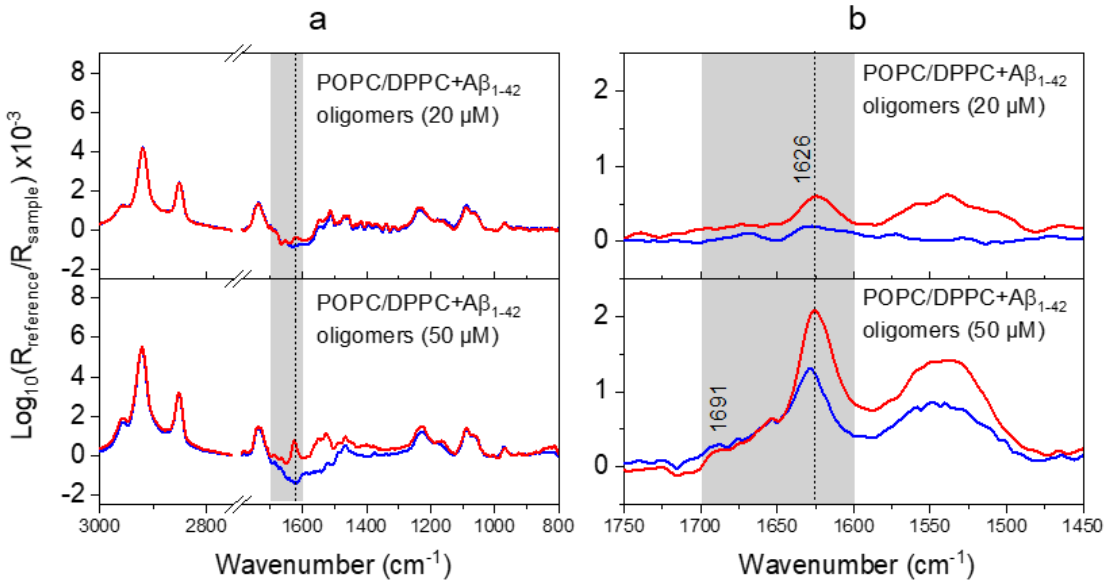

Figure 6. ATR-FTIR spectra of POPC/DPPC SLBs afterwards exposed for two hours to $A\beta_{1-42}$ under oligomers form at 20 µM (upper boxes), at 50 µM (bottom boxes). (a) Reference spectrum is the HEPES buffer. (b) Reference spectrum is the SLB before the exposure to $A\beta_{1-42}$, spectra in the amide bands region. Red curves: before rinsing with HEPES buffer. Blue curves: after rinsing with HEPES buffer. ν: stretching, a: antisymmetric, s: symmetric. The grey rectangle is used to highlight the amide I band region in every spectrum.

The spectra in the amide I region showed several bands at 1626, 1648, 1676 and 1695 cm^{-1} assigned to β-sheets, α-helices/random, β-turn and antiparallel β-sheet structures, respectively

(Figure 6b). These spectral features were consistent with the occurrence of Aβ oligomers.[33] A dramatic decrease in the intensities of the amide bands was observed after rinsing with the HEPES buffer (Figures 6b and S6), showing the high decrease of $A\beta_{1-42}$ concentration at the vicinity of the SLBs upon rinsing. In addition, after rinsing, (1) the amide I band maximum shifted from 1625-1626 to 1629-1630 cm^{-1}, (2) the relative contribution of bands at higher wavenumbers (1648-1695 cm^{-1}) was higher, and (3) the overall width at half height was higher. These features suggested that the rinsing step removed the bigger oligomers.[43-44] S_L calculated from νsCH_2 bands (Table S1) before exposure and after 2 hours of exposure and the rinsing step with HEPES buffer increased from 0.26 to 0.42 for DOPC/DPPC SLBs whereas it remained stable for pure POPC SLBs and increased from 0.32 to 0.50 for pure DPPC SLB. These results suggested that the presence of $A\beta_{1-42}$ oligomers affected weakly the structure of POPC domains, whereas the impact on DPPC domains was significantly higher and increased the SLB ordering.

DISCUSSION

Despite the continuous efforts to study AD, the underlying causes and mechanisms leading to its development remain frustratingly elusive. The lack of fundamental knowledge with regard to AD-inducing molecular mechanisms can partially explain the dramatic absence of any efficient therapy. The need to frame new hypotheses from basic research has become as imperative as the need to gain a better understanding of these mechanisms. Current approaches focus on the characterization of phenomena associated with what are considered initial, intermediary or final stages of the disease during the alteration of neuronal membranes by neurotoxins derived from extracellular forms of Aβ peptide, identified as a specific component of the fibrils of amyloid plaques. Aβ peptide is above all a membrane protein, originating from segments of both the juxtamembrane and transmembrane domains of APP

and as such necessitates its characterization in the context of the membrane to better ascertain its physicochemical behavior. Aβ oligomers (especially $A\beta_{1-42}$) are considered as neurotoxic. To date the most popular hypothesis for the amyloidogenic pathway postulates that Aβ monomers are first expelled from the membrane, then oligomerize before they either insert back into or adsorb onto the cell membrane and thereby accumulate and initiate the cytotoxic cascade.[2] We here investigate by a multidisciplinary approach an alternative hypothesis in which a subpopulation of nascent Aβ stays in membranes immediately following proteolysis of APP by γ-secretase, giving rise to possible Aβ oligomerization directly within the cell membrane.

We first built a physiologically relevant model of nascent $A\beta_{1-42}$, positioned in the bilayer based on a micellar structure of APPjmtm (2LOH), not only respecting the insertion depth but also the initial secondary structure of the transmembrane alpha-helix of the $A\beta_{1-42}$ peptide. Atomistic MD simulations of this nascent $A\beta_{1-42}$ model revealed a post-cleavage form of the peptide that remains stably inserted in the model phospholipid bilayer, with a tendency to conserve the intramembrane α-helical secondary structure. These results are original and pertinent, despite previous reports of MD simulations inserted in bilayers. At first view, our MD results resemble another $A\beta_{1-42}$ simulation work, in which a different model of α-helical $A\beta_{1-42}$, also positioned in a lipid bilayer, remained stably anchored in lipid bilayers, with a flexible N-terminal interacting with the solvent while its C-terminal remained embedded in membrane in an α-helical conformation.[16] However, the insertion depth used by the authors places the extra- and juxtamembrane sequences of $A\beta_{1-42}$ directly within the bilayer, contrary to our model. In our case, we matched insertion depth of the transmembrane helix to that of the NMR APPjmtm structure (2LOH), which we used as a template to construct $A\beta_{1-42}$.[15] Several MD studies using various initial helical Aβ structures (featuring important differences with our $A\beta_{1-42}$ model) inserted in membranes reported the peptides also

adsorbing on the bilayer surface.[46-48] Notably in Zhao *et al.*,[48] Aβ is shown to adsorb on the membrane surface with loss of α-helical secondary structure when simulation was carried out with three peptides embedded in a cholesterol and DPPC bilayer. On the contrary, we show that systems containing two and four Aβ peptides in DOPC remained anchored. This difference in results may be attributed to the fact that the initial structure used by Zhao *et al.*[48] had been obtained in solution whereas the structure used here as a template was resolved in micellar form, thus providing a physicochemical environment more analogous to a lipid bilayer. These discrepancies in results underline the importance of the proper selection and insertion depth of initial structures.

Biological cell membranes have a much more complex organization than the simple models of lipid bilayers studied here.[49] However, DPPC and POPC phospholipids are the most prominent in neuronal cell membranes and are commonly used as main components of cell membrane models.[28, 50] They form bilayers with liquid-phase and gel-phase domains suitable therefore for a first approximation of "raft-like domains". Accordingly, SLBs made of POPC and DPPC in this work aimed at verifying experimentally the predictions from MD simulations. MD calculations give the initial situation of the system just after cleavage of CTFβ by γ-secretase, whereas physicochemical experiments on the SLBs address their state when the peptide is not only monomeric but mostly oligomerized (Figure 1). Between the two time-scales, there is a gap corresponding to the peptide oligomerization (Figure 7).

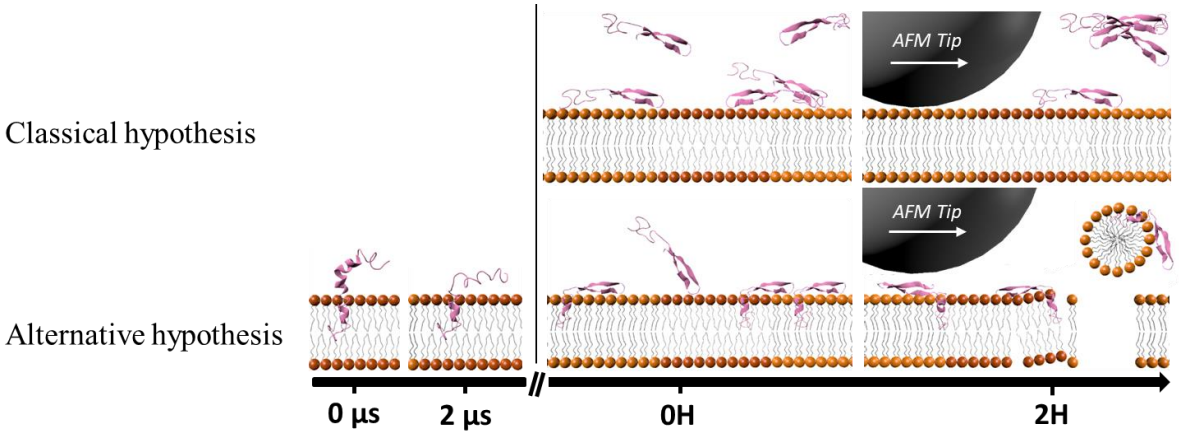

Figure 7. Time-scale discrepancy between theoretical and experimental measurements. Schematic representation of SLB time-evolution in the presence of free and embedded $A\beta_{1-42}$ peptides. Over short time-scale (i.e., less than 2 μs), embedded $A\beta_{1-42}$ peptides adopt an α-helix conformation in their transmembrane domain. Over long time-scale (i.e., from minutes to 2 hours), free $A\beta_{1-42}$ peptides form oligomers with β-sheet conformation. Embedded $A\beta_{1-42}$ under initial monomeric form adopts an α-helix and a random conformation. AFM imaging allows to observe the possible degradation induced par the presence of the peptide in the SLB. Arrows indicate the movement direction of the AFM tip.

We evidenced through experiments that $A\beta_{1-42}$ monomers and oligomers remained embedded in POPC/DPPC SLBs when $A\beta_{1-42}$ molecules are pre-assembled with phospholipids to make the SLB (POPC/DPPC/$A\beta_{1-42}$) as previously shown for a brain lipid extract bilayer.[41] The integration of $A\beta_{1-42}$ was very low when oligomers are considered. ATR-FTIR indicated that $A\beta_{1-42}$ is present in the membranes when incorporated in the SLB during its formation. Yet the signal was too low to accurately determine its secondary structure in the presence of oligomers, but a helical structure was detected when monomers are considered. The incorporation of oligomers leads to a brittle SLB with pores located mainly in POPC liquid phase areas, whereas few cracks were observed in the DPPC gel-phase. Protofibril-like structures were detected mainly in the POPC liquid phase as revealed by the AFM images. It is in accordance with a study where it was shown that the SLB fluidity can affect the $A\beta_{1-42}$ fibrillation process.[51] The fluid phase facilitates the fibrillation by a high mobility of $A\beta_{1-42}$ molecules, whereas the $A\beta_{1-42}$ molecules adsorbed on the gel phase have a less mobility that retard the fibrillation. Pores seemed also delimited by $A\beta_{1-42}$ protofibrils (Figure 3c). $A\beta_{1-42}$ oligomers remain anchored to the bilayers for several hours. The SLBs then exhibited numerous damages and mechanical fragility compared to the SLB devoid of

$A\beta_{1-42}$. The POPC liquid-phase areas were weakened by $A\beta_{1-42}$ oligomers, as it is shown by the pores in this liquid phase of the SLB. Our results indicated that the small amount of $A\beta_{1-42}$ oligomers finally integrated within the membrane is sufficient to cause significant damages in membrane structure and organization. This effect is strengthened by aging (Figure S11) as damages are more numerous in both fluid and gel phases.

The p3 peptide, a fragment of $A\beta_{1-42}$, is synthetized through the non-amyloidogenic pathway with the help of α- and γ-secretases. Considering the fact that the extramembrane domain of p3 is twice shorter than the one of $A\beta_{1-42}$, it should be better anchored within the SLB. Indeed, MD calculations predict that the p3 monomer also stays into the membrane (Figure S5). Accordingly, we constructed a SLB with preassembled phospholipids and p3 peptide (denoted POPC/DPPC/p3). The AFM images on such SLB did not show any alteration of the POPC/DPPC/p3 SLB (Figure S8) conversely to what was observed for $A\beta_{1-42}$. As p3 peptide is not considered neurotoxic[3] and it did not alter the structure of the SLB, the damages originated from $A\beta_{1-42}$ when within the SLB should be linked to its toxicity. In accordance with our results, Bokvist et al.[52] reported that monomeric $A\beta_{1-40}$ incorporation leads to a stable helical structure of the transmembrane domain (12 amino acids). However, the extracellular domain was composed of a middle helix and a β-hairpin that can adopt easily a β-sheet conformation. Our MD calculations showed that the conformation of the extracellular domain of monomeric $A\beta_{1-42}$ is rather random, which can evolve in more structured conformations (Figure 1).

On the contrary, $A\beta_{1-42}$ only loosely adsorbs onto beforehand POPC/DPPC SLB, forming later growing aggregates mostly located on DPPC gel phase. Such AFM observations are in line with the infrared spectra. If free $A\beta_{1-42}$ peptides enter the SLB, it will be highly concentrated at the vicinity of the investigated surface, leading to an enhanced signal with respect to peptide concentration even at 20 µM.[53] Neither pores nor defects within the bilayer

were observed on AFM images. Exposure of preformed SLBs to $A\beta_{1-42}$ was limited to a simple adsorption of $A\beta_{1-42}$ aggregates preferentially on the DPPC gel-phase, and they were easily removed either by a slight increase in the applied scanning force in AFM imaging or by rinsing with HEPES buffer as shown in ATR-FTIR experiments. In addition, very low disorganization of the SLBs was measured. AFM and ATR-FTIR measurements strongly suggested that free $A\beta_{1-42}$ oligomers were not able to insert into the SLBs. The accumulation of small $A\beta_{1-42}$ aggregates on DPPC gel phase domains was already observed, and it was suggested that the rigid gel phase domains may act as platforms to concentrate peptide and enhance its aggregation. It may be relevant to studies that implicate lipid rafts in Aβ accumulation and toxicity.[29] Pore formation has also been reported in the case of Aβ deposited on pure DPPC bilayers,[30] and fibrils of 2-nm apparent height were reported with Aβ deposited on bilayers of DOPC with cholesterol.[26, 31] However, this is the first time that occurrence of pores, fibrils and oligomers deposits on a same phospholipid bilayer is reported.

Some works suggested that cholesterol may play a significant role in AD.[54] Similar experiments to those described above were performed with SLBs containing 14% (molar) cholesterol. POPC/DPPC/cholesterol/$A\beta_{1-42}$ SLB or POPC/DPPC/cholesterol SLB then exposed to $A\beta_{1-42}$ oligomers were also analyzed by AFM imaging and ATR-FTIR spectroscopy (Figures S9-S10, Table S1). The same conclusions can be drawn: whereas the POPC/DPPC/cholesterol/$A\beta_{1-42}$ SLB showed pores as for POPC/DPPC/$A\beta_{1-42}$ SLB, no or very weak alteration of the POPC/DPPC/cholesterol SLB was observed when $A\beta_{1-42}$ was added after the building of the SLB.

CONCLUSION

Taken together, the results of our multidisciplinary approach confirm that possibly $A\beta_{1-42}$ may be membrane-bounded after its release by the γ-secretase. The presence of $A\beta_{1-42}$

monomers or oligomers into model membranes composed of POPC and DPPC (i.e. when $A\beta_{1-42}$ monomers or oligomers were self-assembled with the lipid bilayer) leads to membrane damage, and thus can support the hypothesis that oligomerization may occur in the membrane, altering it, and inducing the first events of AD mechanisms.

MATERIALS and METHODS

Theoretical and computational simulations.

Dimeric APPjmtm NMR structure was obtained from Protein Data Bank (PDB: 2LOH). This structure spans the entire transmembrane domain of $A\beta_{1-42}$, but lacks 14 residues on its N-terminal.[15] We constructed these 14 residues using SWISS-MODEL. CHARMM-GUI Bilayer Builder web-interface was used to prepare all systems.[55] $A\beta_{1-42}$ N-terminus were acetylated. 13 residues on C-terminal were manually removed from the PDB file, and no capping was selected in CHARMM-GUI (NONE option). N-terminal was acetylated (ACE option) in simulations with two peptides and protonated (NTER) in systems with one and four peptides. Peptides protonation state was computed using PROPKA3 at pH 7. $A\beta_{1-42}$ peptides were placed in a DOPC phospholipid bilayer and solvated in water. Peptides were oriented so that the vector between Cα of residues 36 and 42 was normal to the bilayer surface. Aβ was embedded so that residue ASN27 was at the same level as phosphate groups of phospholipids. Water thickness on each side of the protein and membrane ensemble was set to 30 Å.

All simulations were performed using GROMACS ver. 2018.3 and CHARMM36 force field with a temperature of 303 K using Noose-Hover thermostat and a pressure of 1 atm using Parinello-Rahman barostat. The time step was 2 fs with leap-frog algorithm integrator. Systems were energy minimized for 5000 steps, then underwent NVT equilibration for 25 ps and NPT equilibrations for 325 ps. During equilibration, position restraint on lipids' phosphorus atoms in Z dimension were gradually removed. One simulation of 2 μs with a

single $A\beta_{1-42}$ peptide, four simulations of 1 μs with two peptides and one simulation of 1.4 μs with four peptides were performed. The four simulations with two peptides started with different orientation of peptides: one was rotated on the membrane surface plan by 0°, 90°, 180° and 270°. In systems containing two peptides, one peptide was translated from its initial position in the Y axis, resulting in a distance of 30 Å between each peptide LYS28 Cα. In systems containing four peptides, two pairs were made with a distance of 15 and 25 Å between each peptide (translated on X axis), and a distance of 35 Å between each pair (translated on Y axis). All simulation analyses were performed using GROMACS and visual molecular dynamics (VMD) Tools. Figures were produced using UCSF ChimeraX.

Chemicals.

1,2-dipalmitoylphosphatidylcholine (POPC, 99%), 1-palmitoyl-2-oleoyl-sn-glycero-3-phosphocholine (DPPC, 99%) cholesterol (99%), and HEPES (99.5%) were purchased from Merck (France). 1,1,1,3,3,3-hexafluoro-2-propanol (HFIP, 99%) was purchased from Aldrich. Chloroform (99.80%) and $CaCl_2$ (99%) were purchased from Prolabo (France). NaCl (99.9%) was purchased from VWR Chemical (Belgium). The HEPES buffer solution was composed of 150 mM NaCl and 20 mM HEPES. HEPES-Ca buffer solution was composed of 150 mM NaCl, 20 mM HEPES, and 2 mM $CaCl_2$. The pH of both buffers was adjusted to 7.4. The $A\beta_{1-42}$ (DAEFRHDSGYEVHHQKLVFFAEDVGSNKGAIIGLMVGGVVIA) and p3 (LVFFAEDVGSNKGAIIGLMVGGVVIA) peptides in powder form were purchased from Proteogenix (Schiltigheim, France) with a purity of > 95%. They were stored at -20°C.

Supported phospholipid bilayers preparation.

Supported lipid bilayers (SLBs) composed of POPC, DPPC, POPC/DPPC, and DPPC/POPC/cholesterol were prepared as it follows. Single lipids or lipid mixtures were

dissolved in $CHCl_3$ in a glass flask, $CHCl_3$ was then evaporated under a N_2 flow. The lipids were dried overnight in a desiccator under vacuum. They were then resuspended from the walls of the glass flask by vigorous vortexing during 1-2 min in HEPES-Ca buffer (10 mL at 1 mM final total lipids concentration). To obtain small unilamellar vesicles (SUVs), the suspension was sonicated to clarity (2 cycles of 2 min) using a Branson Digital Sonifier 450 (Branson Ultrasonics Corporation, Danbury, USA) at 60% of maximal power while keeping the suspension in an ice bath to limit heating. The suspension was finally filtered on 0.2 µm nylon filters (Whatman Inc., USA) to eliminate titanium particles from the ultrasound probe. The SLBs were obtained according to the vesicle fusion method. For AFM experiments, the SUV solution was put into contact with a freshly cleaved mica substrate for 60 min at 65 °C. Then pre-heated (65°C) filtered HEPES buffer solution was added onto the mica substrate and the samples were slowly cooled down to room temperature. Finally, the samples were carefully rinsed to remove SUV excess using HEPES buffer. Samples were transferred into the AFM fluid cell while avoiding dewetting. For ATR-FTIR experiments, SLB were built-up directly onto an ATR diamond crystal hosted in a homemade closed flow cell. The lipids solutions were pumped using a peristatic pump (Gilson Minipuls3) and put in contact with the pre-heated ATR diamond crystal (65°C). After one hour, filtered HEPES-Ca buffer pre-heated at 65°C was added to the flow cell prior to cool down gradually the system from 65°C to 25°C during 1.5 hours. At 25°C, the SLB formed onto the ATR diamond crystal was rinsed with a flow of HEPES buffer to remove excess SUV. During the whole procedure, biochemical fingerprint of the lipids and the SLB was monitored by recording infrared spectra according the procedure specified below.

Free $A\beta_{1-42}$ aqueous solutions.

For studies with $A\beta_{1-42}$ as oligomers, the desired quantity of a 221 µM stock solution (1 g/L) of the peptide in HEPES was diluted to obtain final concentrations of 2.5 µM, 20 µM or 50 µM. For studies with $A\beta_{1-42}$ mainly as monomers, 1 mg of $A\beta_{1-42}$ was dissolved in 1 mL hexafluoroisopropanol (HFIP) and kept under agitation during 1 h 30 (vortex then shaker and finally vortex, for 20, 60 and 10 minutes, respectively). HFIP was then evaporated under a gentle stream of N_2, and then put under vacuum during 3 hours to ensure total evaporation of HFIP. $A\beta_{1-42}$ as obtained was afterwards dissolved in chloroform or in HEPES buffer for further study. The conformational structure of the peptide was checked by infrared spectroscopy before further use.

Deciphering the interactions of free $A\beta_{1-42}$ with SLBs.

For AFM experiments, the desired quantity of a 221 µM $A\beta_{1-42}$ solution in HEPES freshly prepared was added to the cell containing the SLB to obtain final concentrations of 2.5 µM or 20 µM of $A\beta_{1-42}$ oligomers. For IR-ATR experiments, a solution of the peptide at a concentration of 20 or 50 µM in HEPES buffer freshly prepared replaced the HEPES buffer into the flow cell.

Model membrane of SLBs constructed in the presence of $A\beta_{1-42}$ or p3 peptide.

One mg of pure $A\beta_{1-42}$ was dissolved in 1 mL chloroform. Selected volumes were added to the lipids at 0.5 mM in chloroform to obtain final concentrations of $A\beta_{1-42}$ at 20 µM or 50 µM, and then chloroform was evaporated. The mixture was resuspended from the walls of the glass flask with HEPES-Ca buffer. SUVs were obtained by sonication of the suspension to clarity according to the procedure described above. The suspension was then filtered on 0.2 µm nylon filters to eliminate titanium particles from the ultrasound probe. Finally, the POPC/DPPC/$A\beta_{1-42}$ SLBs were formed onto either mica or diamond according to the protocol

described above. For experiments including p3 peptide, the same procedure was followed dissolving one mg of pure p3 in 1 mL chloroform and the selected volume was added to the lipid before chloroform evaporation to reach a final concentration of 20 µM. For aging samples, SLBs were kept in the fridge at 4°C during 7 days, in buffer medium, before being imaged again with the AFM at 25°C.

Atomic Force microscopy (AFM).

AFM images were recorded using a Bioscope Resolve (Bruker France SAS, Palaiseau, France) operating in PeakForce-Quantitative Nano-Mechanical (PeakForce QNM) imaging mode. Silicon nitride probes with a nominal spring constant of 0.12 N/m and nominal tip radius of 1 nm were purchased from Bruker (PeakForce-HIRS-SSB tips, Bruker France SAS). Topography images were performed in liquid (HEPES buffer) at 25°C with a resolution of 512 × 512 pixels, a scan rate of 0.6 Hz, and a maximal applied force of 0.4 nN for the study of SLBs. The maximal applied force has been increased up to 1.2 nN during image scanning to evaluate the adherence strength between $A\beta_{1\text{-}42}$ aggregates and SLBs. Morphology measurements were performed in independent triplicates by recording at least 5 images for each SLBs composition.

The root-mean-square roughness (RMS or Rq) of each domain of mixed SLBs (*i.e.* POPC and DPPC domains) was evaluated from AFM images using NanoScope Analysis (version 1.19) software. RMS was calculated for each domain area as a function of *N* and *M* where *N* is the resolution of the selected area (*i.e.* the number of points per line), and *M* is the number of lines in the area. RMS is given by the standard deviation of the *z*-values (amplitude) determined for each point of coordinates (*x*, *y*) in the image according to the following equation:

$$\text{RMS}\ (N,M) = \sqrt{\frac{1}{NM}} \sum_{x=1}^{N} \sum_{y=1}^{M} (z(x,y) - \bar{z}(N,M))^2 \qquad (1)$$

Statistical comparisons were performed using the ANOVA test according to the Kruskal-Wallis method, the latter test being implemented in SigmaPlot (version 12) software. The average size of filamentous structures was determined by measurements on 30 structures.

Infrared spectroscopy.

Attenuated Total Reflection Fourier Transform infrared (ATR-FTIR) spectra were recorded between 4000 and 700 cm^{-1} on a Bruker Vertex 70v spectrometer (Wissembourg, France) equipped with a MCT detector cooled with liquid N_2. A GladiATR (Pike Technologies) accessory mounted with a diamond crystal (incident light at 45°, one reflection) in a plate with a temperature controller was used. Non-polarized spectra were recorded with 100 scans, whilst polarized spectra were recorded with 200 scans, both with a spectral resolution of 4 cm^{-1}. To remove the contribution of water vapor, the sample compartment was purged by a flow of N_2. All spectra are presented in an absorbance scale corresponding to $Log_{10}(R_{reference}/R_{sample})$ where R is the internal reflectance of the device. The reference was, according to the experiment, the HEPES buffer solution or the SLB with sole lipids in HEPES buffer medium. OPUS software (version 7.8) drives the spectrometer. Before further analysis, the baseline of the spectra was corrected at the following points: 3585, 3024, 2790, 1800 and 850 cm^{-1}. Bands integrated intensities were measured on the following regions: νsCH_2: 2880-2823 cm^{-1}, $\nu C{=}O$: 1766-1700 cm^{-1}, Amide I: 1646-1603 cm^{-1}, Amide II: 1536-1511 cm^{-1}. Every experiment presented is representative of at least two independently conducted measurements.

The CH_2 stretching region (2800-3000 cm^{-1}) was used to obtain an estimation of phospholipid composition in the POPC/DPPC SLBs at 25°C. Spectra were fitted with Lorentzian Features of individual bands from pure POPC and pure DPPC SLB spectra were first determined from spectra recorded at 25°C. Spectra of the mixed SLB (POPC/DPPC) were then fitted with the

band parameters determined beforehand. This procedure allowed calculating the contributions of both phospholipids, and to reach the composition of the SLB.

ASSOCIATED CONTENT

Supporting Information.

It contains additional additional results on MD calculations, AFM and IR-ATR data are included in the Supporting Information file named Siniscalco_et_al_SI.pdf. The file is available free of charge.

AUTHOR INFORMATION

Corresponding author

* fabienne.quiles@univ-lorraine.fr

Laboratoire de Chimie Physique et Microbiologie pour les Matériaux et l'Environnement (LCPME, UMR 7564), 405, rue de Vandœuvre, F-54600 Villers-lès-Nancy, France.

Author contributions

LP and MT designed the hypotheses and the MD part of the project. DS performed the AFM and IR-ATR experiments. SKB, OL and LP performed the simulations. DS, GF and FQ analyzed the experimental data. All authors discussed the data and drew the interpretations. FQ, GF, DS, LP and MT wrote the manuscript. All authors have read the manuscript and brought improvement to it.

Funding Sources

This work was performed thanks to a Mirabelle+ grant from Lorraine Université d'Excellence (LUE).

ACKNOWLEDGMENTS

FQ, GF and DS thank the Spectroscopy and Microscopy Service Facility (SMI) of LCPME (Université de Lorraine-CNRS – https://www.lcpme.ul.cnrs.fr/equipements/smi/) where the IR-ATR and AFM experiments were performed. Molecular graphics and analyses were performed thanks to UCSF ChimeraX, developed by the Resource for Biocomputing, Visualization, and Informatics at the University of California, San Francisco, with support from National Institutes of Health R01-GM129325 and the Office of Cyber Infrastructure and Computational Biology, National Institute of Allergy and Infectious Diseases. The authors also thank N. Szluc for help on the optimisation of the protocol for obtaining $A\beta_{1-42}$ monomers in chloroform.

REFERENCES

1. Dickson, T. C.; Vickers, J. C., The Morphological Phenotype of beta-Amyloid Plaques and Associated Neuritic Changes in Alzheimer's Disease. *Neuroscience* **2001,** *105* (1), 99-107.

2. Cline, E. N.; Bicca, M. A.; Viola, K. L.; Klein, W. L., The Amyloid-β Oligomer Hypothesis: Beginning of the Third Decade. *Journal of Alzheimer's disease : JAD* **2018,** *64* (s1), S567-s610.

3. Arbor, S. C.; LaFontaine, M.; Cumbay, M., Amyloid-beta Alzheimer Targets - Protein Processing, Lipid Rafts, and Amyloid-beta Pores. *The Yale journal of biology and medicine* **2016,** *89* (1), 5-21.

4. Andrew, R. J.; Kellett, K. A. B.; Thinakaran, G.; Hooper, N. M., A Greek Tragedy: The Growing Complexity of Alzheimer Amyloid Precursor Protein Proteolysis. *J. Biol. Chem.* **2016,** *291* (37), 19235-19244.

5. Kawarabayashi, T.; Shoji, M.; Younkin, L. H.; Wen-Lang, L.; Dickson, D. W.; Murakami, T.; Matsubara, E.; Abe, K.; Ashe, K. H.; Younkin, S. G., Dimeric Amyloid β Protein Rapidly Accumulates in Lipid Rafts followed by Apolipoprotein E and Phosphorylated Tau Accumulation in the Tg2576 Mouse Model of Alzheimer's Disease. *The Journal of Neuroscience* **2004,** *24* (15), 3801-3809.

6. Evrard, C.; Kienlen-Campard, P.; Coevoet, M.; Opsomer, R.; Tasiaux, B.; Melnyk, P.; Octave, J. N.; Buée, L.; Sergeant, N.; Vingtdeux, V., Contribution of the Endosomal-Lysosomal and Proteasomal Systems in Amyloid-β Precursor Protein Derived Fragments Processing. *Front Cell Neurosci* **2018,** *12*, 435.

7. Rajendran, L.; Annaert, W., Membrane Trafficking Pathways in Alzheimer's Disease. *Traffic* **2012,** *13* (6), 759-770.

8. Colin, J.; Thomas, M. H.; Gregory-Pauron, L.; Pinçon, A.; Lanhers, M. C.; Corbier, C.; Claudepierre, T.; Yen, F. T.; Oster, T.; Malaplate-Armand, C., Maintenance of Membrane Organization in the Aging Mouse Brain as the Determining Factor for Preventing Receptor Dysfunction and for Improving Response to Anti-Alzheimer Treatments. *Neurobiol Aging* **2017,** *54*, 84-93.

9. Bode, D. C.; Baker, M. D.; Viles, J. H., Ion Channel Formation by Amyloid-β42 Oligomers but Not Amyloid-β40 in Cellular Membranes. *J. Biol. Chem.* **2017,** *292* (4), 1404-1413.

10. Fabiani, C.; Antollini, S. S., Alzheimer's Disease as a Membrane Disorder: Spatial Cross-Talk Among Beta-Amyloid Peptides, Nicotinic Acetylcholine Receptors and Lipid Rafts. *Frontiers in Cellular Neuroscience* **2019,** *13*, 309.

11. Beel, A. J.; Sakakura, M.; Barrett, P. J.; Sanders, C. R., Direct Binding of Cholesterol to the Amyloid Precursor Protein: An Important Interaction in Lipid-Alzheimer's Disease Relationships? *Biochim. Biophys. Acta* **2010,** *1801* (8), 975-982.

12. Allinquant, B.; Clamagirand, C.; Potier, M.-C., Role of Cholesterol Metabolism in the Pathogenesis of Alzheimer's Disease. *Current Opinion in Clinical Nutrition & Metabolic Care* **2014,** *17* (4), 319-323.

13. Fernandez, M. A.; Biette, K. M.; Dolios, G.; Seth, D.; Wang, R.; Wolfe, M. S., Transmembrane Substrate Determinants for γ-Secretase Processing of APP CTFβ. *Biochemistry* **2016,** *55* (40), 5675-5688.

14. Colvin, M. T.; Silvers, R.; Ni, Q. Z.; Can, T. V.; Sergeyev, I.; Rosay, M.; Donovan, K. J.; Michael, B.; Wall, J.; Linse, S.; Griffin, R. G., Atomic Resolution Structure of Monomorphic Aβ42 Amyloid Fibrils. *J. Am. Chem. Soc.* **2016,** *138* (30), 9663-9674.

15. Nadezhdin, K. D.; Bocharova, O. V.; Bocharov, E. V.; Arseniev, A. S., Dimeric Structure of Transmembrane Domain of Amyloid Precursor Protein in Micellar Environment. *FEBS Lett.* **2012,** *586* (12), 1687-92.

16. Poojari, C.; Strodel, B., Stability of Transmembrane Amyloid β-Peptide and Membrane Integrity Tested by Molecular Modeling of Site-Specific Aβ42 Mutations. *PLoS One* **2013,** *8* (11), e78399-e78399.

17. Baumann, K. N.; Šneiderienė, G.; Sanguanini, M.; Schneider, M.; Rimon, O.; González Díaz, A.; Greer, H.; Thacker, D.; Linse, S.; Knowles, T. P. J.; Vendruscolo, M., A Kinetic Map of the Influence of Biomimetic Lipid Model Membranes on Aβ42 Aggregation. *ACS chemical neuroscience* **2023,** *14* (2), 323-329.

18. Niu, Z.; Zhang, Z.; Zhao, W.; Yang, J., Interactions between Amyloid β Peptide and Lipid Membranes. *Biochimica et Biophysica Acta (BBA) - Biomembranes* **2018,** *1860* (9), 1663-1669.

19. Liu, R. Q.; Zhou, Q. H.; Ji, S. R.; Zhou, Q.; Feng, D.; Wu, Y.; Sui, S. F., Membrane Localization of beta-Amyloid 1-42 in Lysosomes: a Possible Mechanism for Lysosome Labilization. *J. Biol. Chem.* **2010,** *285* (26), 19986-96.

20. Sardar Sinha, M.; Ansell-Schultz, A.; Civitelli, L.; Hildesjö, C.; Larsson, M.; Lannfelt, L.; Ingelsson, M.; Hallbeck, M., Alzheimer's Disease Pathology Propagation by Exosomes Containing Toxic Amyloid-beta Oligomers. *Acta Neuropathol* **2018,** *136* (1), 41-56.

21. Österlund, N.; Luo, J.; Wärmländer, S.; Gräslund, A., Membrane-Mimetic Systems for Biophysical Studies of the Amyloid-β Peptide. *Biochimica et biophysica acta. Proteins and proteomics* **2019,** *1867* (5), 492-501.

22. Clifton, L. A.; Campbell, R. A.; Sebastiani, F.; Campos-Terán, J.; Gonzalez-Martinez, J. F.; Björklund, S.; Sotres, J.; Cárdenas, M., Design and Use of Model Membranes to Study Biomolecular Interactions using Complementary Surface-Sensitive Techniques. *Adv. Colloid Interface Sci.* **2020,** *277*, 102118.

23. Attwood, S. J.; Choi, Y.; Leonenko, Z., Preparation of DOPC and DPPC Supported Planar Lipid Bilayers for Atomic Force Microscopy and Atomic Force Spectroscopy. *Int J Mol Sci* **2013,** *14* (2), 3514-39.

24. Azouz, M.; Cullin, C.; Lecomte, S.; Lafleur, M., Membrane Domain Modulation of Aβ1–42 Oligomer Interactions with Supported Lipid Bilayers: an Atomic Force Microscopy Investigation. *Nanoscale* **2019,** *11* (43), 20857-20867.

25. Jacquot, A.; Francius, G.; Razafitianamaharavo, A.; Dehghani, F.; Tamayol, A.; Linder, M.; Arab-Tehrany, E., Morphological and Physical Analysis of Natural Phospholipids-Based Biomembranes. *PLoS One* **2014,** *9* (9), e107435.

26. Drolle, E.; Hane, F.; Lee, B.; Leonenko, Z., Atomic Force Microscopy to Study Molecular Mechanisms of Amyloid Fibril Formation and Toxicity in Alzheimer's Disease. *Drug metabolism reviews* **2014,** *46* (2), 207-23.

27. Smeralda, W.; Since, M.; Cardin, J.; Corvaisier, S.; Lecomte, S.; Cullin, C.; Malzert-Fréon, A., β-Amyloid Peptide Interactions with Biomimetic Membranes: A Multiparametric Characterization. *Int. J. Biol. Macromol.* **2021,** *181*, 769-777.

28. Drolle, E.; Negoda, A.; Hammond, K.; Pavlov, E.; Leonenko, Z., Changes in Lipid Membranes May Trigger Amyloid Toxicity in Alzheimer's Disease. *PLoS One* **2017,** *12* (8), e0182194.

29. Choucair, A.; Chakrapani, M.; Chakravarthy, B.; Katsaras, J.; Johnston, L. J., Preferential Accumulation of Aβ(1−42) on Gel Phase Domains of Lipid Bilayers: An AFM and Fluorescence Study. *Biochimica et Biophysica Acta (BBA) - Biomembranes* **2007,** *1768* (1), 146-154.

30. Hane, F.; Drolle, E.; Gaikwad, R.; Faught, E.; Leonenko, Z., Amyloid-β Aggregation on Model Lipid Membranes: an Atomic Force Microscopy Study. *Journal of Alzheimer's disease : JAD* **2011,** *26* (3), 485-94.

31. Drolle, E.; Gaikwad, R. M.; Leonenko, Z., Nanoscale Electrostatic Domains in Cholesterol-Laden Lipid Membranes Create a Target for Amyloid Binding. *Biophys. J.* **2012,** *103* (4), L27-L29.

32. Lewis, R. N. A. H.; McElhaney, R. N., Membrane Lipid Phase Transitions and Phase Organization Studied by Fourier Transform Infrared Spectroscopy. *Biochimica et Biophysica Acta (BBA) - Biomembranes* **2013,** *1828* (10), 2347-2358.

33. Sarroukh, R.; Goormaghtigh, E.; Ruysschaert, J. M.; Raussens, V., ATR-FTIR: a "Rejuvenated" Tool to Investigate Amyloid Proteins. *Biochim. Biophys. Acta* **2013,** *1828* (10), 2328-38.

34. Sarroukh, R.; Cerf, E.; Derclaye, S.; Dufrêne, Y. F.; Goormaghtigh, E.; Ruysschaert, J.-M.; Raussens, V., Transformation of Amyloid β(1–40) Oligomers into Fibrils is Characterized by a Major Change in Secondary Structure. *Cell. Mol. Life Sci.* **2011,** *68* (8), 1429-1438.

35. Goormaghtigh, E.; Raussens, V.; Ruysschaert, J. M., Attenuated Total Reflection Infrared Spectroscopy of Proteins and Lipids in Biological Membranes. *Biochim. Biophys. Acta* **1999,** *1422* (2), 105-85.

36. Tamm, L. K.; Tatulian, S. A., Infrared Spectroscopy of Proteins and Peptides in Lipid Bilayers. *Q. Rev. Biophys.* **1997,** *30* (4), 365-429.

37. Korshavn, K. J.; Satriano, C.; Lin, Y.; Zhang, R.; Dulchavsky, M.; Bhunia, A.; Ivanova, M. I.; Lee, Y.-H.; La Rosa, C.; Lim, M. H.; Ramamoorthy, A., Reduced Lipid Bilayer Thickness Regulates the Aggregation and Cytotoxicity of Amyloid-β. *J. Biol. Chem.* **2017,** *292* (11), 4638-4650.

38. Lee, J.; Kim, Y. H.; F, T. A.; Gillman, A. L.; Jang, H.; Kagan, B. L.; Nussinov, R.; Yang, J.; Lal, R., Amyloid β Ion Channels in a Membrane Comprising Brain Total Lipid Extracts. *ACS chemical neuroscience* **2017,** *8* (6), 1348-1357.

39. Ewald, M.; Henry, S.; Lambert, E.; Feuillie, C.; Bobo, C.; Cullin, C.; Lecomte, S.; Molinari, M., High Speed Atomic Force Microscopy to Investigate the Interactions between Toxic Aβ(1-42) Peptides and Model Membranes in Real Time: Impact of the Membrane Composition. *Nanoscale* **2019,** *11* (15), 7229-7238.

40. Jeong, J. S.; Ansaloni, A.; Mezzenga, R.; Lashuel, H. A.; Dietler, G., Novel Mechanistic Insight into the Molecular Basis of Amyloid Polymorphism and Secondary Nucleation during Amyloid Formation. *J. Mol. Biol.* **2013,** *425* (10), 1765-1781.

41. Mrdenovic, D.; Majewska, M.; Pieta, I. S.; Bernatowicz, P.; Nowakowski, R.; Kutner, W.; Lipkowski, J.; Pieta, P., Size-Dependent Interaction of Amyloid β Oligomers with Brain Total Lipid Extract Bilayer—Fibrillation Versus Membrane Destruction. *Langmuir* **2019,** *35* (36), 11940-11949.

42. Aguilar, M.-I.; Hou, X.; Losic, D.; Mechler, A.; Martin, L.; Small, D., Single-Molecule Imaging of Amyloid-β Protein (Aβ) of Alzheimer's Disease. In *Bio-nanoimaging. Protein Misfolding and Aggregation*, Uversky, V. N.; Lyubchenko, Y. L., Eds. Academic Press: 2014; pp 47-56.

43. Shivu, B.; Seshadri, S.; Li, J.; Oberg, K. A.; Uversky, V. N.; Fink, A. L., Distinct β-Sheet Structure in Protein Aggregates Determined by ATR-FTIR Spectroscopy. *Biochemistry* **2013,** *52* (31), 5176-83.

44. Benseny-Cases, N.; Cócera, M.; Cladera, J., Conversion of Non-Fibrillar beta-Sheet Oligomers into Amyloid Fibrils in Alzheimer's Disease Amyloid Peptide Aggregation. *Biochem. Biophys. Res. Commun.* **2007,** *361* (4), 916-21.

45. Bisceglia, F.; Natalello, A.; Serafini, M. M.; Colombo, R.; Verga, L.; Lanni, C.; De Lorenzi, E., An Integrated Strategy to Correlate Aggregation State, Structure and Toxicity of Aß 1–42 Oligomers. *Talanta* **2018,** *188*, 17-26.

46. Miyashita, N.; Straub, J. E.; Thirumalai, D., Structures of beta-Amyloid Peptide 1-40, 1-42, and 1-55-the 672-726 Fragment of APP-in a Membrane Environment with Implications for Interactions with gamma-Secretase. *J. Am. Chem. Soc.* **2009,** *131* (49), 17843-52.

47. Liguori, N.; Nerenberg, P. S.; Head-Gordon, T., Embedding Aβ42 in Heterogeneous Membranes Depends on Cholesterol Asymmetries. *Biophys. J.* **2013,** *105* (4), 899-910.

48. Zhao, L. N.; Chiu, S. W.; Benoit, J.; Chew, L. Y.; Mu, Y., Amyloid β Peptides Aggregation in a Mixed Membrane Bilayer: a Molecular Dynamics Study. *J. Phys. Chem. B* **2011,** *115* (42), 12247-56.

49. van Meer, G.; Voelker, D. R.; Feigenson, G. W., Membrane Lipids: Where they Are and How they Behave. *Nature reviews. Molecular cell biology* **2008,** *9* (2), 112-124.

50. Åkesson, A.; Lind, T.; Ehrlich, N.; Stamou, D.; Wacklin, H.; Cárdenas, M., Composition and Structure of Mixed Phospholipid Supported Bilayers Formed by POPC and DPPC. *Soft Matter* **2012,** *8* (20), 5658-5665.

51. Yang, M.; Wang, K.; Lin, J.; Wang, L.; Wei, F.; Zhu, J.; Zheng, W.; Shen, L., Gel Phase Membrane Retards Amyloid β-Peptide (1–42) Fibrillation by Restricting Slaved Diffusion of Peptides on Lipid Bilayers. *Langmuir* **2018,** *34* (28), 8408-8414.

52. Bokvist, M.; Lindström, F.; Watts, A.; Gröbner, G., Two Types of Alzheimer's beta-Amyloid (1-40) Peptide Membrane Interactions: Aggregation Preventing Transmembrane Anchoring versus Accelerated Surface Fibril Formation. *J. Mol. Biol.* **2004,** *335*, 1039-49.

53. Quiles, F.; Saadi, S.; Francius, G.; Bacharouche, J.; Humbert, F., In Situ and Real Time Investigation of the Evolution of a *Pseudomonas fluorescens* Nascent Biofilm in the Presence of an Antimicrobial Peptide. *Biochim. Biophys. Acta, Biomembr.* **2016,** *1858* (1), 75-84.

54. Penke, B.; Paragi, G.; Gera, J.; Berkecz, R.; Kovács, Z.; Crul, T.; VÍgh, L., The Role of Lipids and Membranes in the Pathogenesis of Alzheimer's Disease: A Comprehensive View. *Curr. Alzheimer Res.* **2018,** *15* (13), 1191-1212.

55. Lee, J.; Cheng, X.; Swails, J. M.; Yeom, M. S.; Eastman, P. K.; Lemkul, J. A.; Wei, S.; Buckner, J.; Jeong, J. C.; Qi, Y.; Jo, S.; Pande, V. S.; Case, D. A.; Brooks, C. L., 3rd; MacKerell,

A. D., Jr.; Klauda, J. B.; Im, W., CHARMM-GUI Input Generator for NAMD, GROMACS, AMBER, OpenMM, and CHARMM/OpenMM Simulations Using the CHARMM36 Additive Force Field. *J. Chem. Theory Comput.* **2016,** *12* (1), 405-13.

Table of Contents